ACS OMEGA

Open Access

http://pubs.acs.org/journal/acsodf

Article

Development and Characterization of Polyethylenimine-Infiltrated Mesoporous Silica Foam Pellets for CO_2 Capture

Ramesh B. Komma[†] and Gregory P. Dillon*[,†]

Cite This: *ACS Omega* 2024, 9, 32881−32892

Read Online

ACCESS | Metrics & More | Article Recommendations | Supporting Information

ABSTRACT: Polyethylenimine (PEI) has been shown to be promising for direct air capture (DAC) of carbon dioxide and has potential for commercial scale-up globally. Laboratory scale processes include multiple steps, such as mixing, solvent extraction, vacuum application, sonication, and various flushes and activation steps. It is critical to properly control these operating parameters to achieve higher capture capacity as a result of the optimized material configuration. This study adopts previously published pelletization processes for PEI-infiltrated mesoporous foam silica (mesoporous silica foam) to uncover the adsorption mechanisms and optimize the associated fabrication steps, such as sonication, to achieve higher sorbent productivity. A high capture capacity was achieved at 46 °C for 75 wt % PEI loading (2.27 mmol/g) followed by PEI_MSF 70 (1.81 mmol/g) and PEI_MSF 80 (1.44 mmol/g). As part of the optimization, sonication parameters of frequency, amplitude, and time were modified for PEI_MSF 75 sorbent, which resulted in the highest uptake capacity of 3.04 mmol/g (sonicated at 40 kHz and a wave amplitude of 50% for 30 s). These preliminary results would tend to prove that sonication energy affects carbon capture capacity, although there is still a lack of understanding regarding the exact underlying mechanism, suggesting the need for further investigation. It is important to note that the present work is focused on the adsorption mechanisms and not desorption or durability of the capture performance. Ongoing research addresses these factors. This paper is intended to establish baseline DAC behavior of a promising capture medium and begins probing the optimization spectrum by considering the effects of sonication energy on adsorption. Ongoing work intends to address potential abbreviations of the full range of process steps and furthers the understanding of kinetics by considering the desorption and resorption attributes.

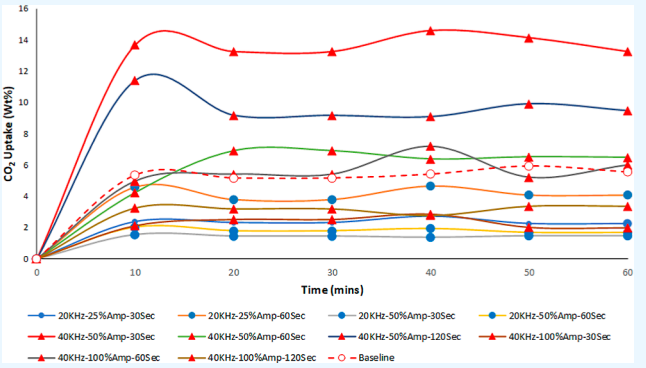

1. INTRODUCTION

Deleterious carbon dioxide (CO_2) emissions have drastically increased over the last century. According to the international energy agency, annual CO_2 emissions from human sources averaged 30 GT over the past 15 years,[1] highlighting the importance of the CO_2 sequestration technology and the urgency of developing scalable systems. The dual challenges of capturing excess CO_2 that has already been emitted and preventing further buildup are equally important. Among the most effective methods explored to date is emissions capture from ambient air using amine sorbents among other media. This is referred to as direct air capture (DAC).

The supported amine groups are an essential class of materials, prominent in separation systems,[1−5] and are shown to be highly effective for reversible CO_2 adsorption.[6,7] Poly ethylenimine [polyethylenimine (PEI)], in particular, has been the most intensively evaluated amine due to the molecular density of amine sites for CO_2 adsorption. Linear and branched PEI of various molecular weights have been studied, and the latter is observed to adsorb more due to a greater variety of viable adsorption sites on the molecular chain. PEI is also available commercially and is generally cost competitive as a medium for capture. Other amines such as polyallylamine and several nonpolymeric amines (diethanolamine, tetraethylenepentamine, and ethylenediamine) have also been evaluated for air capture applications, with varying degrees of success and apparent viability for scale up.[9−18]

The amine CO_2 adsorption efficiency increases when the amines are supported on a solid pore structure, such as silica, metal−organic frameworks, cellulose, and hydrogels, to create solid-supported amines.[8−17] Predominantly, mesoporous silica is used to support amines due to its good thermal stability, high pore volume, and abundance of surface silica hydroxyl groups.[18,19] A particularly useful model silica system is SBA-15 (Santa Barbara Amorphous), a mesoporous silica foam (MSF) system. It has well-ordered and monodisperse pores, arranged

Received: April 15, 2024
Revised: July 5, 2024
Accepted: July 11, 2024
Published: July 20, 2024

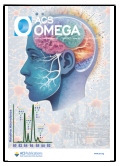

as a hexagonal lattice of parallel cylinders[20,21] that are favorable for incorporation of PEI. This system can be further configured into mesostructured cellular foam (MCF) silica powder which has largely uniform cells and windows; the cells are in spherical 3D form creating a large pore system. Following infiltration of the MSF with PEI, the material is carbonated before pelletization to produce robust, dry composite materials. This pretreatment step helps conversion of the liquid phase PEI into a carbamate solid phase.[22] Finally, the developed tablet shape offers the potential for loading into various configurations and system locations for a wide spectrum of CO_2 capture applications. The authors believe that the MSF system used in this study and the MCF materials used in prior work are very similar. The distinction is in the resultant pore geometry, brought about through the use of a swelling agent in the synthesis of MCF. However, the relative surface areas and chemical characters are virtually identical.

The authors noted that the preparation method suggested in prior work by Knowles et al.[24] for MCF is a highly variable process which may nonetheless be improved in several ways. The presented preparation methods take about 14−15 days to produce useable pellets. The fabrication method includes infiltration of solvent borne PEI into the MSF, mechanical stirring, sonication, rotary evaporation, alternating series of N_2 purges and evacuations, carbonation, and finally pelletizing. Transferring materials while executing these extended procedures can increase the scope for error and lead to variable quality and effectiveness of the resultant pellets. The work presented here is the first stage of an effort to evolve a resource and time-efficient procedure that applies the pellet production methods presented by Knowles and others to advance the technology toward effective practical implementation. The ideal composition and morphology of pellets are yet to be established, and mechanisms to control the exact loadings and distributions of the active polymer adsorption sites have not been determined. It has been shown that there is an inverse correlation between the loading of the polymer and CO_2 uptake capacity, logically hypothesized to be related to the free surface area to volume ratio.[23]

The present study explored the effect of a lower loading of PEI in MSF-based pellets than previously published on the CO_2 uptake capacity. The study followed an established procedure described by Knowles[24] but was changed according to onsite facilities. The study extends the loading of the PEI below 80% pore volume equivalents which was previously concluded to be the best composition[23] for the MCF system, and it was believed that with application of effective sonication and a lower polymer loading, higher CO_2 uptake would result. Therefore, it was decided to lower the PEI loading to 70 and 75% pore volume equivalents. The CO_2 uptake was determined for the three baseline materials of loadings (70, 75, and 80 wt %), and measurements were conducted to fully characterize the material in efforts to understand the underlying mechanisms that control the adsorption performance. It is now hypothesized that there is an effective trade-off between polymer loading, and therefore surface area supplying adsorption sites, and ability to access and coat the entire pore network. Essentially, there may be an upper limit on viable loading, imposed by the potential blockage of the nanometer scale pores. Environmental scanning electron microscopy (ESEM) and Fourier transform infrared spectroscopy in attenuated total reflectance (FTIR-ATR) mode were applied in the study, providing data that have not been previously reported.

This study also focused on optimizing the sonication step in the fabrication process by controlling the parameters of frequency, sonication time, and amplitude, which is hypothesized to enhance the infiltration of PEI. Following identification of the best-performing polymer loading (75 wt %), several additional samples were fabricated for which the baseline process (that applied a 2.5 h sonication step at 10 kHz) was modified to be applied by direct sonication. The preliminary results suggest a measurable effect of sonication on the uptake capacities of the sorbent, and scanning electron microscopy shows that improved performance may be due to modification of the pore network.

2. EXPERIMENTAL SECTION

2.1. Materials and Material Synthesis. The three PEI baseline material loadings were prepared using a pelletization method presented by Knowles.[22,23] The MSF carrier medium was acquired from ACS Materials, under the trade name SBA 15. This material is a porous silica powder, with a reported particle diameter range of 0.5−2 μm, pore diameters of 6−13 nm, and a pore volume of 1−2 cm^3/g. The branched PEI polymer with a molecular weight of 1200 g/mol was acquired from Sigma-Aldrich. Using these materials, three different pore volume fill equivalents (targeted equivalents 80, 75, and 70%) of branched PEI were prepared by measuring 71.2, 70, and 68.8 wt %, respectively, of PEI polymer relative to the carrier weight and pore volume. They are the baseline materials denoted as PEI MSF 70, PEI MSF 75, and PEI MSF 80, respectively. The values were calculated based on the published pore volume of the silica and the densities of both materials.

The MSF silica (∼1 g) was loaded with the PEI via wet infiltration from an ethanol solution. The baseline materials were sonicated using a Soniclean sonicator for 2 h and 30 min after which they were mechanically agitated by a magnetic stirrer for 24 h. This sonication method applied on the baseline materials as suggested in prior work is referred to as indirect sonication, as shown in Figure S1 (Supporting Information). The bulk solvents were later removed by rotary evaporation using a rotavapor under vacuum at 40 °C (Figure S2 Supporting Information). The samples were flushed with dry N_2 for 4 days and then evacuated for 5 days at 110 °C via a Schlenk line (temperature controlled by immersion of round-bottomed flasks in an oil bath). Samples were then activated by repurging with N_2 and again evacuated for 24 h at 110 °C. The activated powder products were carbonated by flushing with pure CO_2 for 24 h at 60 °C. The resultant powder samples were compressed into 10 mm diameter pellets by application of 8.12 t for 10 min at room temperature, as shown in Figure S3. The samples were seen to be well consolidated and possessed sufficient structural integrity to allow the application of the various material characterization methods.

As part of the process optimization for the long fabrication procedure, the influence of the sonication step was studied in depth. All samples were then subjected to the same sample production methods as the baseline materials except for the sonication step. The prior work suggests that the sonication process aids infiltration, although the authors of the present work did not find specific published data supporting this contention. It was believed that this was an inefficient sonication method since several sites of energy attenuation

https://doi.org/10.1021/acsomega.4c03551
ACS Omega 2024, 9, 32881−32892

existed between the transducer and the sample solution. Nonetheless, it is believed that the application of ultrasonic wave energy is reasonable since associated pressure waves may produce a "pumping" effect that would improve infiltration into nanoscale pores, provided the amplitude and frequency effectively allow coupling of the energy at the appropriate length scale. This is likely to be somewhere between the diameter of the MSF powder and the nanopore diameter. Therefore, a group of bulk solutions of PEI MSF 75 were sonicated using Sonics hand-held horns delivering 20 and 40 kHz (500 W and 15 A) of ultrasonic energy. Maximum amplitudes for these ultrasonic horns are on the order of 115 μm, though the delivered energy is dependent on the frequency, with the higher frequency providing approximately half of the delivered amplitude. Samples were sonicated for varying times and adjusted amplitudes, by the direct method represented in Figure S1. In this case, the ultrasonic energy is delivered directly into the solution, with significant associated turbulence and measurable, though modest, increase in temperature.

The experimental arrangement used for the sonication steps is shown in Figure S4. The schedule of the sonication treatments is shown in Table 1. The amplitude is expressed as a percentage of the maximum that could be delivered with each ultrasonic horn. Note that it is not possible to determine the exact amplitude of sonication since the probe is embedded in the solution and fluid damping effects cannot be precisely measured. The subsequent purging and activation steps required a "ganging" arrangement (Supporting Information—Figure S5) to ensure consistency, in which the flushing process was completed by creating a plenum, from which the purging or activating gases could be delivered equally to each of the dried powders.

Table 1. Sonication Parameters Applied to Prepare the MSF PEI Pellets

sonication conditions	frequency (kHz)	amplitude (%)	time (s)
baseline	10		10,800
20 kHz 25% Amp 30 s	20	25	30
20 kHz 25% Amp 60 s	20	25	60
20 kHz 50% Amp 30 s	20	50	30
20 kHz 50% Amp 60 s	20	50	60
40 kHz 50% Amp 30 s	40	50	30
40 kHz 50% Amp 60 s	40	50	60
40 kHz 50% Amp 120 s	40	50	120
40 kHz 100% Amp 30 s	40	100	30
40 kHz 100% Amp 60 s	40	100	60
40 kHz 100% Amp 120 s	40	100	120

2.2. Material Characterization. Before characterization techniques were applied, the prepared pellets were placed in a vacuum oven at 105 °C for 14 h to remove any gases that may have been adsorbed during the fabrication process. Scanning electron microscopy images were taken on an FEI Quanta 650 ESEM. Two types of samples were prepared. The first set was made by fracturing the samples with a hammer blow at room temperature and collecting the pieces for fractographic analysis. This procedure was repeated for the second set, except that the samples were immersed in liquid nitrogen for 2 min before hammer fracture. The Quanta ESEM allows the beam column parameters to be adjusted, based on the sample properties. Therefore, gold coating was not used since the beam voltage and column pressure could be adapted (by introduction of water vapor) for imaging adjustment. It should be noted that a sample that is likely desorbing CO_2 during examination is an imaging challenge that requires environmental column control. It is not believed that adequate imaging of these types of samples can be completed using conventional scanning electron microscopy.

For the baseline materials, infrared (IR) spectra were obtained using a single-reflection diamond ATR accessory of a Bruker Vertex 70 spectrometer/Hyperion 300 imager. FTIR data were recorded between 4000 and 400 cm^{-1} at a resolution of 4 cm, and 16 scans were averaged for each spectrum at room temperature. Also, for the baseline materials, N_2 adsorption at 77 K data of two samples in the pellet form and the MCF silica were collected by using Micromeritics TriStar 3020 and Micromeritics ASAP 2040 adsorption analyzers. These data were used to estimate the specific surface area and the mesopore volume for the baseline materials using the

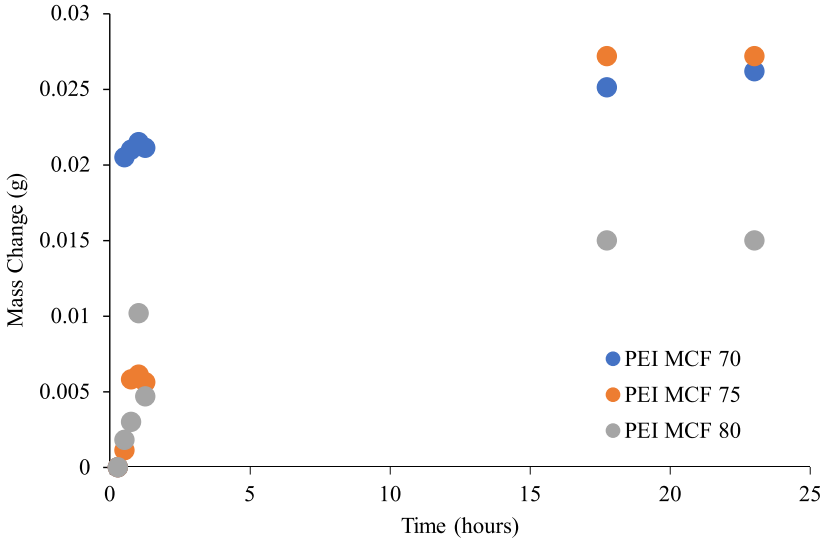

Figure 1. Breakthrough curves for various loading levels of PEI in MSF pellets.

https://doi.org/10.1021/acsomega.4c03551
ACS Omega 2024, 9, 32881−32892

Brunauer–Emmett–Teller (BET) method[24] and the Barrett–Joyner–Halenda method,[25] respectively. Estimations of surface area were made by application of the BET equations to adsorption data points over the range of 0.05–0.15 p/p_0, and mesopore volumes were estimated as the volume of N_2 retained during desorption at p/p_0 = 0.90. The true densities of the materials were found via helium pycnometry using a Micromeritics AccuPyc 1340.

2.3. CO_2 Adsorption Measurement Procedure. To find the percent adsorption of CO_2, the pellets were first loaded into rubber septum-covered glass vials submerged in an oil bath set at 45 °C. Carbon dioxide flushing was completed through a Schlenk line at constant pressure and gas flow verified through an oil bubbler. The change in mass was calculated by weighing the glass vials on a Fisher Scientific XA Analytical Balance every 15 min for the first 1.5 h and then again after 17 h and 45 min and 23 h. The following process was used to calculate the CO_2 uptake:

Mass change

$$\text{change in mass (g)}: A - B$$

where mass of (glass vial + gas in the vial + rubber stopper + pellet) = A, mass of (glass vial + gas in the vial + rubber stopper) = B.

CO_2 uptake

$$\text{PEI}_{\text{MSF}}x = \frac{\text{change in mass (g)}}{0.04401\text{g/mmol}} = A = \frac{A \text{ in mmol}}{\text{initial weight of the pellet in grams}} = B \text{ mmol/g}$$

x—percentage of PEI loaded (70, 75, 80), A—mmol of change in mass, B—final CO_2 uptake per g of pellet, and note: molecular weight of CO_2 = 0.04401 g/mmol.

3. RESULTS AND DISCUSSION

Results are presented and discussed in three broad categories: (1) CO_2 adsorption measurement, (2) general characterization of sorbents, and (3) scanning electron microscopy.

3.1. CO_2 Adsorption. *3.1.1. Baseline Process Materials.* The breakthrough curves shown in Figure 1, plotted for the adsorption of CO_2, were generated using data collected at 46 ± 0.5 °C, following evaluations suggested in prior work.[23] Note that these samples were produced using the indirect sonication method, applied for 2 h and 30 min. The associated data are given in Table 2 with the asymptotic CO_2 uptake values given in Table 3.

PEI MSF 75 achieved the highest uptake of 2.27 mmol/g, followed by PEI MSF 70 with 1.81 mmol/g and finally PEI MSF 80 at 1.44 mmol/g. The data for PEI MSF 80 fall in the range of previously reported uptake capacity[23] for MCF systems. However, the uptake capacity data reported here break a linear trend as different loadings of PEI do not correspond to the uptake rates. Note that the data in Figure 1 show the change in uptake compared to the 15 min values. This approach was adopted for clarity since the adsorption process involves the introduction of the CO_2 through the Schlenk line, and the earlier part of the process is characterized by stabilization of the uptake mechanism. The rate of uptake was highest in the first hour, and each sample had a specific associated time over which a rapid uptake was seen. In all instances, the great majority of the uptake was complete after about 18 h, reaching an apparent saturation point (asymptote) in approximately 1 day. Earlier studies have suggested that the PEI phase may simply be blocking the pore openings rather than filling the pores completely. This is supported by the investigations of Holewinski et al.[26] which suggested that the pore filling of SBA-15 silica occurs differently in the case of sorbents with low and high PEI loadings. When low amounts of PEI are loaded onto the silica support, PEI forms a coating on the pore walls. When the PEI content is increased beyond a critical value, it is suggested that the polymer agglomerates, forming superficial plugs of approximately the same diameter that do not extend through the length of the pore. Increasing the PEI loading above 80 wt % resulted in no additional uptake capacity, tending to confirm the contention of the existence of a critical loading level. Based on the prior studies and the data reported here, this seems to occur between 75 and 80 wt %. The adsorption data correlate with the apparent architecture of the material supported, as captured in the ESEM study. Not only are the PEI MSF 75 pores more evenly distributed than the MSF PEI 80 and MSF PEI 70 samples but they also exhibit a more consistent geometry.

3.1.2. Variable Sonication Process Materials. The uptake capacity of the pellets subjected to variable sonication for adsorption of CO_2 is summarized in Table 4 and is presented

Table 2. Raw CO_2 Uptake Data for MSF Silica Gel Infiltrated with Various Mass Loadings of PEI

	Δmass/g		
time (min)	PEI MSF 70	PEI MSF 75	PEI MSF 80
15	0.37	0.33	0.87
30	0.39	0.33	0.87
45	0.39	0.34	0.87
60	0.39	0.34	0.88
75	0.39	0.34	0.87
1065	0.39	0.36	0.88
1380	0.39	0.36	0.88

Table 3. Final CO_2 Uptake Data for MSF Silica Infiltrated with Various Mass Loadings of PEI

sample	final CO_2 uptake (mmol/g)
PEI MSF 70	1.81
PEI MSF 75	2.27
PEI MSF 80	1.44

Table 4. Overall Average CO_2 Uptake Capacity in Both wt % and per mmol/g Pellet

sonication conditions	CO_2 uptake (wt %)	CO_2 capacity (mmol/g)
baseline (10 kHz)	5.45	2.15
20 kHz25% Amp 30 s	2.38	1.20
20 kHz 25% Amp 60 s	4.18	1.60
20 kHz 50% Amp 30 s	1.48	0.99
20 kHz 50% Amp 60 s	1.83	1.24
40 kHz 50% Amp 30 s	13.71	3.04
40 kHz 50% Amp 60 s	6.25	1.09
40 kHz 50% Amp 120 s	9.71	1.74
40 kHz 100% Amp 30 s	2.33	1.64
40 kHz 100% Amp 60 s	5.72	2.13
40 kHz 100% Amp 120 s	3.20	1.50

https://doi.org/10.1021/acsomega.4c03551
ACS Omega 2024, 9, 32881–32892

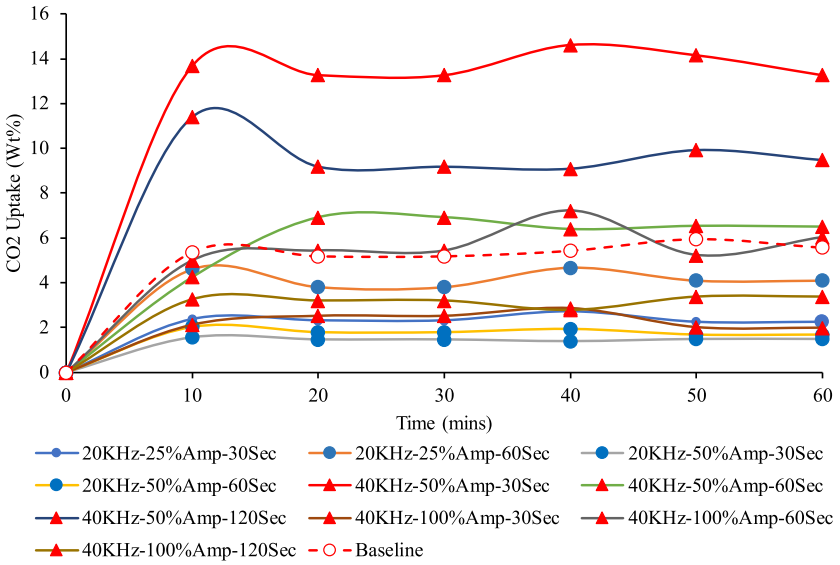

Figure 2. Summary of average CO_2 uptake for all sonicated pellets normalized by respective wt %.

graphically in Figure 2. The data support the primary hypothesis of a significant effect on the CO_2 adsorption by the application of different sonication treatments. The baseline pellet has an adsorption capacity of 2.15 mmol/g which is consistent with values reported by Knowles et al. for MCF. It is critical to compare the results to the baseline performance because this is an established uptake value. A noticeable trend is seen for the CO_2 uptake in Figure 2, which shows a steep uptake for the first 10 min and a slight drop in the next 10 min. Note that the lines are notional polynomial fits to the experimental data and are included only as a visual aid to differentiating between results from different experimental conditions. Fluctuations may indicate transient release of adsorbed gas and readsorption until "locked in" the silica mesopores. Sonicating at 40 kHz and 50% amplitude for 30 s provides the highest capture capacity of 3.04 mmol/g, significantly higher than previously reported values. Pellets processed at 50% amplitude for 30 s and at 20 kHz resulted in the lowest capture capacity of 0.99 mmol/g. The CO_2 capture capacity generally drops significantly when sonicating at 20 kHz relative to 40 kHz, irrespective of the changing amplitude and time of sonication. From the results above, there is an observable influence of varying sonication parameters, and this established the motivation for identifying a critical condition that would lead to optimal energy coupling, resulting in greater capture capacity.

3.1.2.1. Effect of Frequency. Ultrasound wave frequency shows a significant impact on the uptake capacity of the pellets when varied between 20 and 40 kHz. The effective coupling of ultrasonic waves introduced into the solution, including that from waves reflected off the sides of the beaker, seems to show an influence on the uptake capacity, suggesting that possible changes to the pore structure and the infiltration of the PEI polymer have occurred. From Figure 3, all the samples tested at a wave frequency of 20 kHz have a lower CO_2 uptake capacity than the baseline. By contrast, the adsorption capacity may be enhanced significantly at a wave frequency of 40 kHz, with some test conditions doubling the uptake. This trend suggests that wave frequency is indeed a sensitive parameter that could alter the overall CO_2 capture performance of the pellets.

3.1.2.2. Effect of the Amplitude. The amplitude of the ultrasound wave shows a positive correlation with the CO_2 capture across both frequencies. The amount of vibration energy generated depends on the amplitude level, but its effect after different applications is inconsistent, as shown in Figure 4. The amplitude varies after application to the solution due to the distance waves travel between the ultrasonic horn and the walls of the beaker being less than 25 mm. It was seen that there was a slight rise in temperature of the solution after sonication was applied. Results show that at wave frequency of 20 kHz, the lower amplitude of 25% shows a better uptake compared to 50%, regardless of the sonication time.

Samples sonicated at 40 kHz for 30 and 120 s show an identical trend. A wave amplitude of 50% outperforms both the baseline and 100%. Amplitude is inversely correlated to CO_2 uptake capacity. However, when sonicated for 60 s, 100% amplitude outperforms the baseline. Overall, there is an effect of changing amplitude on the CO_2 uptake capacity, and the highest rate is at 50% amplitude for 30 s and at 40 kHz.

3.1.2.3. Effect of Sonication Time. Sonication time is related to the infiltration time over which the walls of mesoporous silica are coated, and this is related to the amount of energy delivered in the system. Increasing the duration of sonication results in reduced capture capacity in three out of four treatments, as shown in Figure 5. Samples sonicated at 40 kHz for 30 s at an amplitude of 50% resulted in the highest capacity, but increasing the duration from 30 to 120 s had a nonlinear effect, which calls into question the effect of sonication time for those specific ultrasonic parameters. Samples sonicated at 40 kHz and 100% amplitude displayed a nonlinear relationship with increasing sonication time and uptake capacity. There is a consistent trend associated with the 20 kHz samples, where increasing the sonication time improved the uptake capacity. Trends in the data presented in Figure 2 through Figure 5 suggest that an asymptotic empirical model can be applied, of the general form

$$\text{uptake} = A - BC^{\text{time}}$$

Figure 6 shows an example curve fit for data generated using the samples subjected to 40 kHz at 50% amplitude for 30 s. The model appears to capture the dynamics of the CO_2 uptake

https://doi.org/10.1021/acsomega.4c03551
ACS Omega 2024, 9, 32881−32892

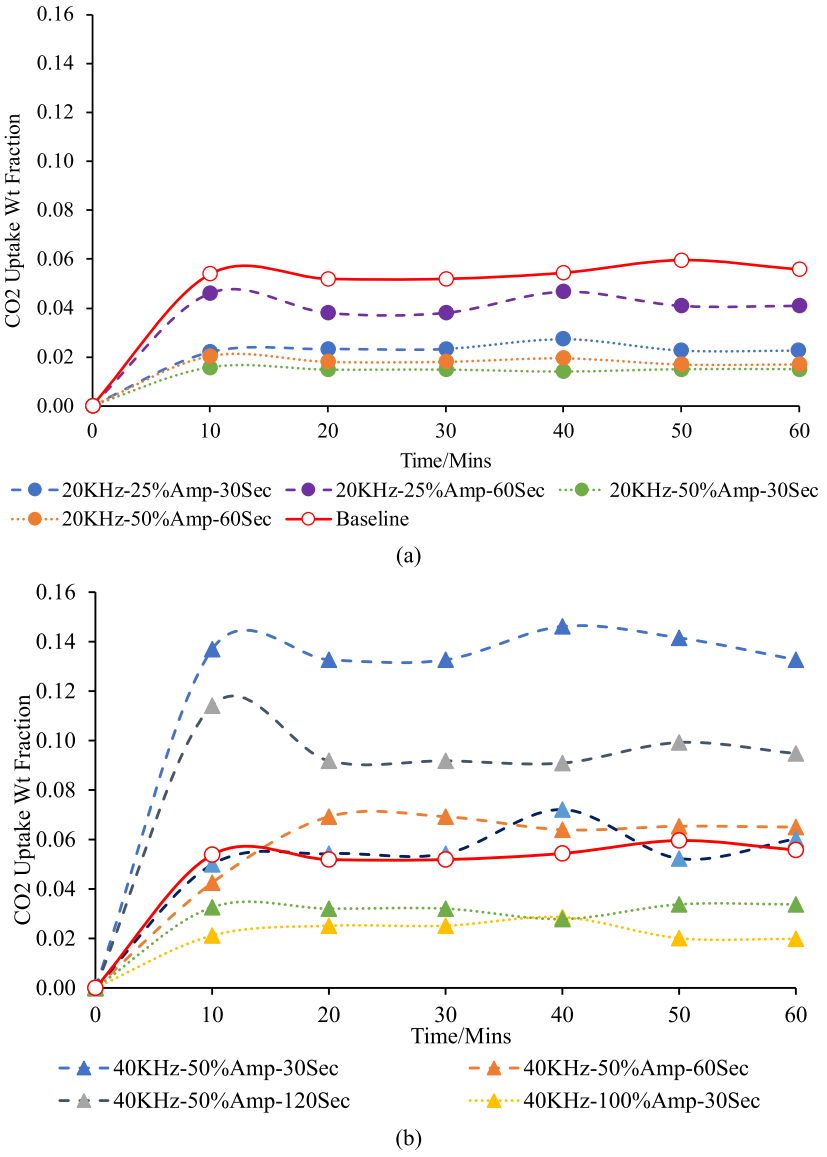

Figure 3. CO_2 uptake capacity measured for pellets sonicated at (a) 20 kHz and (b) 40 kHz. Graphs indicate the effect of sonication frequency on uptake capacity.

very well. The complete set of model fit parameters for all sonication conditions is given in Supporting Information—Table S1.

3.2. General Characterization. Table 5 summarizes the characterization data for the three baseline sample pellet types. The MSF data were developed to understand the basic pore geometries and densities of the materials. The results calculated from helium pyrometer data present an inverse proportional relationship between the loadings of the PEI and the true densities of the materials. They are consistent with the nominal densities of an amine of ∼1.03 and 2.4−2.6 g/mL for silica but are noted to be higher than previously reported.[24] The increase in density could be due to an increased pore volume, which aligns with the surface area and porosity analyzer data. There is a greater apparent surface area and volume than that in previously reported studies, likely due to the lower compaction pressure applied in consolidating the pellets in the current study (10 tons in prior work and 8.2 tons in the current study). Note that ongoing work looks to establish the impact of consolidation pressure on the infiltration and subsequent CO_2 uptake. The measured pore diameter is in the nominally reported range of 2−50 nm for all samples.

The PEI density estimates were calculated from the following equation

$$(\text{true density of MSF})x + \text{given density of PEI}(1 - x) = \text{true density of pellet}$$

3.3. Pellet Macro and SEM Morphology. *3.3.1. Baseline Materials.* Figure S6 (Supporting Information) shows examples of the pellets used in determination of the CO_2 uptake, confirming that they were of uniform size, and on average 4−5 pellets could be made per batch of 2 g powder formulation. The pellets were brittle, firm, and hard. A few fractured when being removed from the pill press. The discoloration of PEI-MCF pellets could be due to minor degradation, though variations in color have been previously reported.[23,24] Samples weighed about 200−400 mg each on average. Figure 7 shows a series of fractographic images

https://doi.org/10.1021/acsomega.4c03551
ACS Omega 2024, 9, 32881−32892

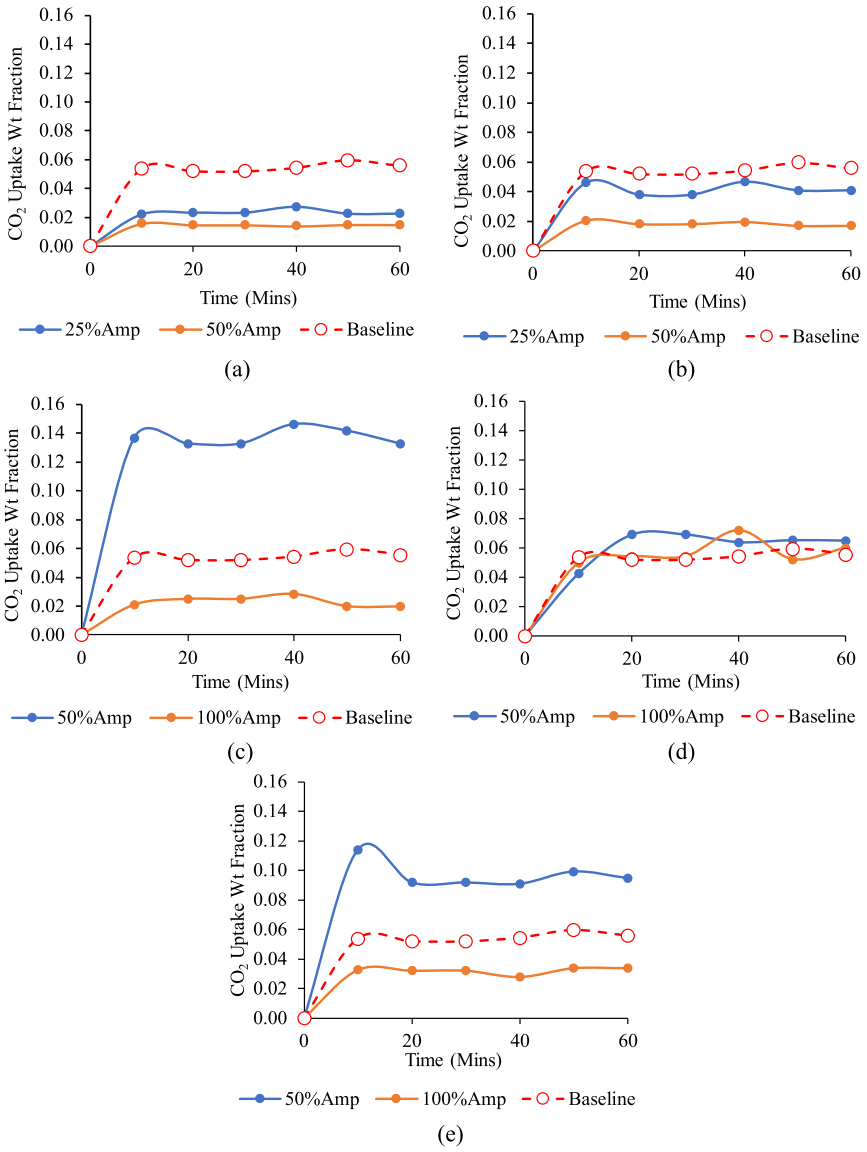

Figure 4. Relationship between amplitude and CO_2 uptake capacity for pellets sonicated at (a) 20 kHz to 30 s, (b) 20 kHz to 60 s, (c) 40 kHz to 30 s, (d) 40 kHz to 60 s, and (e) 40 kHz to 120 s.

generated by room-temperature impact fractures of the three baseline material formulations. It is acknowledged that the quality of the images is variable. This is believed to be due to the release of gaseous materials desorbing from the surface when vacuum is applied in the ESEM beam column, most likely previously adsorbed CO_2. These were imaged on an ESEM which allows control of column conditions (beam voltage and chamber pressure) for better imaging. Consistently, across the loadings, it is evident from the images that well compacted and well-defined infiltration has been achieved, as observed at intermediate magnifications (12,000×). The surface character of the material appears to get denser with higher loadings as less free space, denoted by the darker areas in the images, is observed. However, this is a subtle effect.

At 24,000× magnification, important differences in the architecture of the three different baseline loadings can be seen. It is assumed that the smoother surfaces are the PEI on the surface of an MSF substrate, and significantly, this does not appear as a linear effect with higher loadings. The long strands of the MSF as presented by ACS (citation to be included) are converted into smaller entities when infiltrated with PEI, which can be seen from the images and those presented in the current work. The observed trend is that the material condenses into smaller entities, and the shape of the structure changes with higher loading. The SEM at 24,000× published earlier[27] confirms a similar morphology of the materials processed in this study. It is not immediately clear what accounts for this morphological change; however, the "out of trend" pore volume and surface area data in Table 5 are consistent with microscopy observations. Note from Table 5 and Figure 1 that the highest equilibrium CO_2 uptake is associated with the lowest pore volume, lowest measured surface area, and an intermediate pore diameter. Note further that the character of the PEI MSF 75 fracture surface is markedly different from those of the nominal 70 and 80% loadings. It is smoother and more planar in character, not exhibiting the open pores and discontinuities of the other materials. With these apparent trends, the likely conclusion is that the CO_2 capture efficiency cannot be directly related to measured pore volume, surface area, PEI loading, or even pore diameter. An important

https://doi.org/10.1021/acsomega.4c03551
ACS Omega 2024, 9, 32881−32892

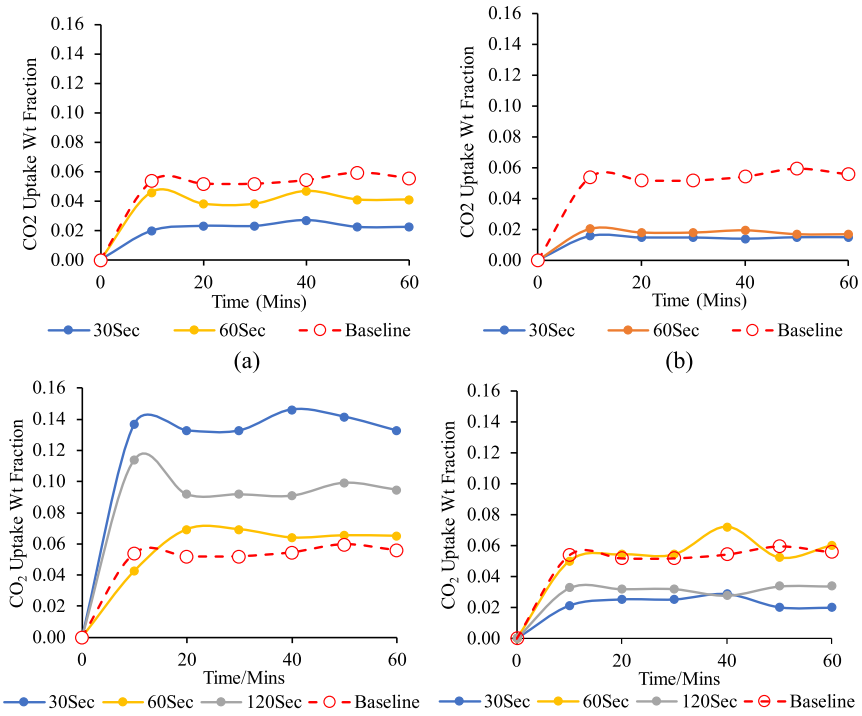

Figure 5. Relationship between sonication time and CO_2 capacity for pellets processed at (a) 20 kHz-25% Amp, (b) 20 kHz-50% Amp, (c) 40 kHz-50% Amp, and (d) 40 kHz-100% Amp.

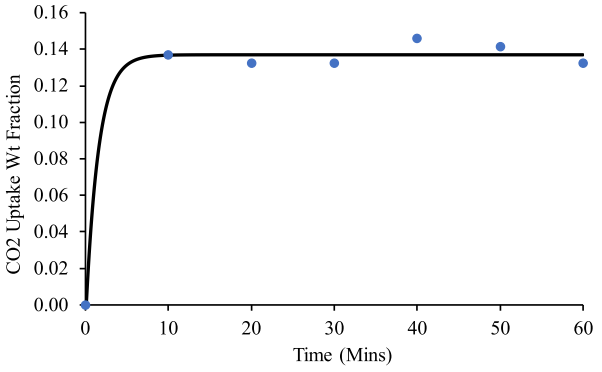

Figure 6. CO_2 uptake data for samples sonicated at 40 kHz and 50% amplitude for 30 s fit to the asymptote model.

Table 5. Characterization Data for Pelletized PEI in MSF Silica

sample	true density (g/cm^3)	Est. PEI loading (%)	BET surface area (m^2/g)	mesopore volume (cm^3/g)	pore diameter (nm)
SBA-15	2.40		550	0.68	6−11
PEI MSF 70	1.69	53.75	107.87	0.29	10.50
PEI MSF 75	1.57	62.81	61.82	0.18	11.82
PEI MSF 80	1.56	63.87	85.44	0.26	11.92

observation from this study is that the pellet morphology is the controlling performance indicator, hence our emphasis on scanning microscopy. It is believed that the capture efficiency is most closely related to the morphology of the carrier medium, and this is based on observations from several fractographic samples, beyond those presented here. Specifically, the more disrupted and "fractured" the SBA structure is the greater the capture efficiency. It is notable from the images, as shown in Figure 7, that the room temperature-generated fracture images are relatively complex, even at magnifications of 24,000×. A second set of samples was freeze fractured using liquid nitrogen, and a typical fracture surface is shown in Figure S7 of the Supporting Information. The bottom of the image shows the molded surface (created by the compaction from the plunger), and the top shows the freeze-fractured surface. The fracture is relatively planar and exhibits a character that is markedly more brittle than that seen with the samples fractured under ambient conditions. Representative fracture surfaces for the three PEI loadings are shown in Figure 8. While the PEI MSF 70 and PEI MSF 80 samples exhibit similar structures, in terms of both the nature of the fractures (brittle) and the morphologies of constituents, the PEI MSF 75 surface is markedly different. In the latter case, the fracture surface is more complex, with areas that may either be associated with agglomeration of PEI (the granular areas can only be the silica powder) or an intermediate morphology of the failure structure. At the time of reporting, the authors do not have a definitive explanation for this fracture characteristic, though again it shows the "out of trend" character of the PEI MSF 75 materials. It may be a random orientation effect, though the difference in character was seen over a relatively wide area of the samples.

As mentioned earlier, inconsistencies and nonlinearities in capture data for this form of material have been reported before, and in some instances, this has been assumed to relate to variations in PEI distributions and plugging of pore networks. The authors contend that the complex fabrication method for pellet production, while logical in its conception and development, is regrettably prone to variation. It is suggested that, for instance, sonication frequency and time could have an impact on the infiltration of the polymer into the MSF spaces and windows. The ultrasonic energy could be a potential key to effective distribution of the polymer as it has

https://doi.org/10.1021/acsomega.4c03551
ACS Omega 2024, 9, 32881−32892

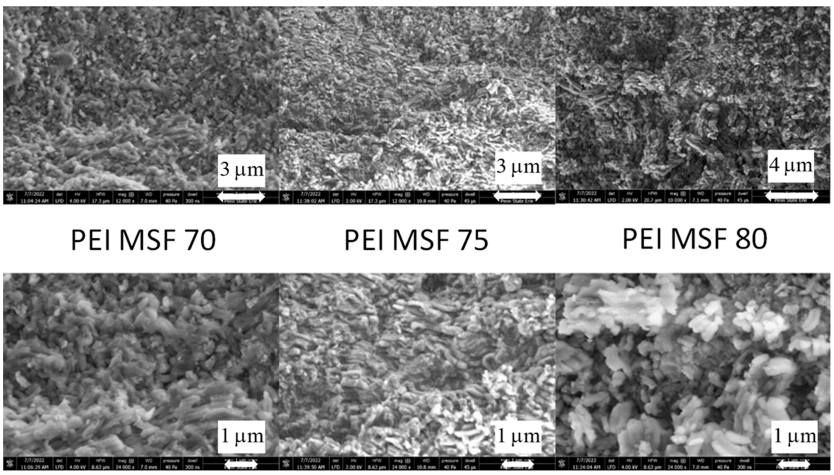

Figure 7. Scanning electron microscopy images of three different loadings of PEI in MSF. The top row images were taken at 12,000× magnification and the bottom row at 24,000×.

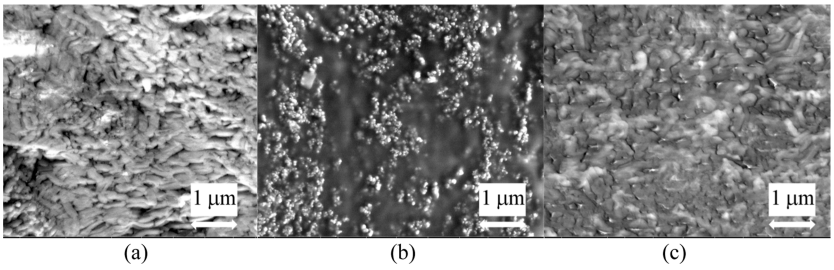

Figure 8. Freeze-fractured surfaces for three loadings: (a) PEI MSF 70, (b) PEI MSF 75, and (c) PEI MSF 80.

been reported that the material produced using sonication has a better CO_2 uptake capacity than that made without this process step.[23] The results from varying frequency of ultrasonic energy has resulted in varying uptake capacities. The ultrasound wave frequency shows a prominent effect on the CO_2 capture of the pellets when varied from 20 to 40 kHz. The intensity of waves introduced into the solution and the resonance of reflected waves from the walls of the container have shown an influence on the uptake capacity, suggesting changes to the pore structure.

3.3.2. Variable Sonication Process Materials. Electron microscopy was conducted to understand the morphological changes attributed to various sonication treatments. It is logical that the arrangement of pores, availability of free space, and infiltration of the polymer determine the capture capacity, when viewed at the micro level. Therefore, the uptake results are cross correlated with ESEM images to study the effect and support the conclusions constructively.

The series of images, as shown in Figure 9, display pellets sonicated at a wave frequency of 40 kHz and 50% amplitude, which yielded the best uptake capacity. Figure 10 shows the uptake trends associated with each of the treatments compared with the baseline formulation. An apparent relationship is observed between the CO_2 uptake capacity and the internal architecture of the pellets. Sonication parameters are believed to allow a coupling effect with the initial structure shown by the published architecture of SBA-15.[28] At 12,000× magnification, it is possible to compare how the CO_2 uptake capacity reduces as the bundles "disappear", possibly agglomerating and reducing the free space. The image for the baseline materials displays fractured/shortened bundles and groupings, altering the arrangement which may be associated with the longer

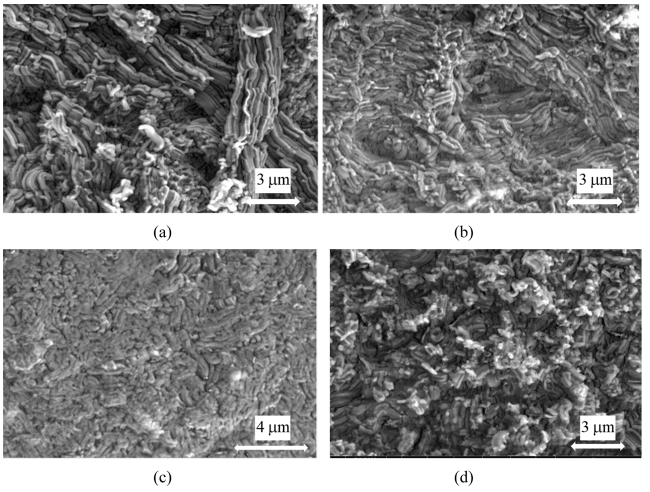

Figure 9. ESEM micrographs of cross-sectional fractured surfaces of (a) 40 kHz-50% Amp-30 s, (b) 40 kHz-50% Amp-120 s, (c) 40 kHz-50% Amp-60 s, and (d) baseline.

sonication time. It can be inferred from the series of images that at a constant amplitude and frequency, the internal pore distribution alters significantly with increased sonication time. The ideal uptake value and morphology show that the raw MSF silica is modified with the infiltration of the polymer, but the internal morphology and free space are very similar to the original pore space. The sample shows a uniform pattern, length of the silica support, and grouping suggestive of the polymer infiltration. This distribution is also reasonable as the samples are subjected to low levels of sonication energy, differing little from the original MSF silica morphology.

https://doi.org/10.1021/acsomega.4c03551
ACS Omega 2024, 9, 32881−32892

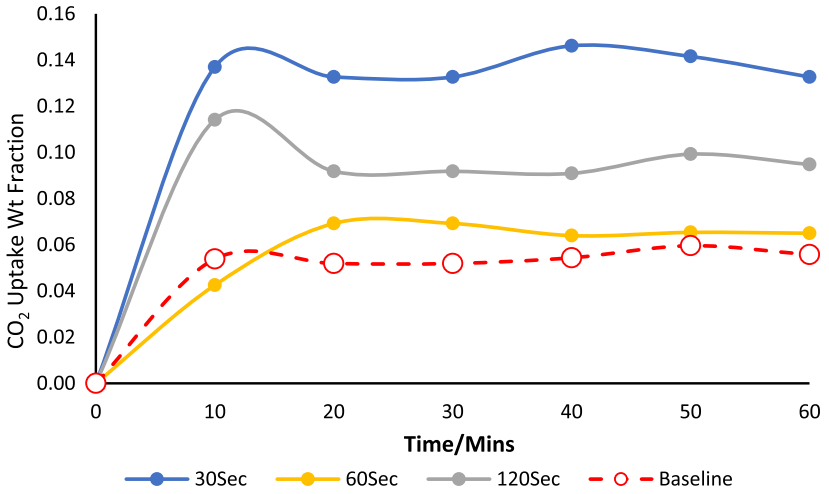

Figure 10. CO_2 adsorption capacity for 40 kHz at 50% amplitude.

By contrast, the series of ESEM images, as shown in Figure 11, indicate a poor architecture and pore geometry, which has a lower capture capacity (Figure 12). When compared with the baseline morphology, it is evident that at 20 kHz, there is less free space with apparent smooth surfaces. An interesting pattern is seen between the pellet morphology of 20 kHz 25% amplitude sonicated for 30 s and the baseline as they look very similar in terms of arrangement and shortened silica bundles as mentioned earlier.

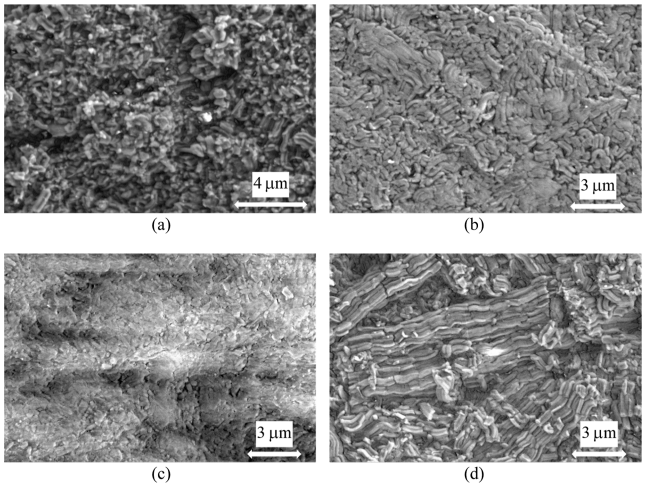

Figure 11. ESEM micrographs of fracture surfaces of pellets sonicated at (a) 20 kHz-25% Amp-30 s, (b) 20 kHz-25% Amp-60 s, (c) 20 kHz-50% Amp-30 s, and (d) 20 kHz-50% Amp-60 s.

FTIR-ATR was used to examine PEI MSF samples with different loadings to confirm successful loading of the CO_2 capture polymer. Figure S8 displays the results from the FTIR spectra, which clearly indicate a successful infiltration of PEI in the MCF. The peaks observed with the pellets precisely correspond to those of MSF and PEI when aligned in the graph. Figure S9 in Supporting Information shows the peak associated with the chemical CO_2 bond which indicates the CO_2 uptake in the pellet. Post combustion gas chromatography was used to record nitrogen levels in the pellet, and it was observed that PEI MSF 75 had the highest at 13.16% followed by PEI MSF 80 (12.30%) and PEI MSF 70 (10.31%). There was a notable higher ratio of CO_2 molecules adsorbed with increased nitrogen. It is observed that PEI MSF 75 had 0.3459

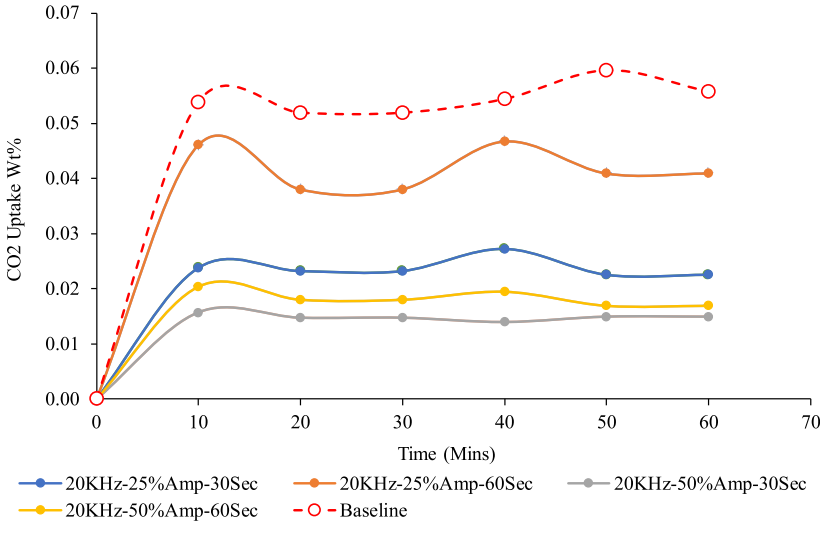

Figure 12. CO_2 adsorption capacity for pellets prepared by sonicating at a frequency of 20 kHz.

https://doi.org/10.1021/acsomega.4c03551
ACS Omega 2024, 9, 32881−32892

of CO_2 per mol of N_2, PEI MSF 80 had 0.1933 of CO_2 per N_2, and PEI MSF 70 had 0.1340 mol of CO_2 per N.

4. CONCLUSIONS AND FUTURE WORK

It is evident from this study that relative to previously published work, there is a lower optimal loading of PEI in MSF-based pellets. PEI MSF 75 achieved the highest uptake of 2.27 mmol/g, followed by PEI MSF 70 with 1.81 mmol/g, and finally PEI MSF 80 at 1.44 mmol/g. The adsorption data correlate with the apparent architecture of the material supported, as captured in the ESEM study. When the PEI content is increased beyond a critical value, it is suggested that the polymer agglomerates, forming superficial plugs in the pore network. Not only are the PEI MSF 75 pores more evenly distributed than the MSF PEI 80 and MSF PEI 70 samples but they also exhibit a more consistent geometry. An important observation from this study is that the pellet morphology is the controlling performance indicator, hence our emphasis on scanning microscopy. The rate of uptake was highest in the first hour and reached a saturation point in approximately 1 day. The key to commercializing the process would be to optimize the entire fabrication in terms of resources and time.

As part of the optimization, sonication parameters of frequency, amplitude, and time were modified for PEI MSF 75 sorbent, which resulted in the highest uptake capacity of 3.04 mmol/g (sonicated at 40 kHz and a wave amplitude of 50% for 30 s). The sonication time was reduced from 2 h 30 min to about 30 s, which highlights the importance of process optimization. Modifying the parameters resulted in a range of uptake capacities from 0.99 mmol/g (sonicated at 20 kHz and a wave amplitude of 50% for 30 s) to 3.04 mmol/g. The CO_2 capture capacity generally drops significantly when sonicating at 20 kHz relative to 40 kHz, irrespective of the changing amplitude and time of sonication. Amplitude is inversely correlated to CO_2 uptake capacity, and the asymptotic empirical model captures the overall dynamic nature of CO_2 uptake. It can be inferred from the series of ESEM images that at a constant amplitude and frequency, the internal pore distribution changes significantly with increased sonication time. The ideal uptake value and morphology show that the raw MSF silica is modified with the infiltration of the polymer, but the internal morphology and free space are very similar to the original pore space. By contrast, the series of ESEM images for the sample with lower capture capacity indicate a poor architecture and pore geometry. There is less free space, with apparent smooth surfaces.

Continuing studies are focused on the overall optimization of the pellet production process. Subtasks of future work will seek to optimize the time and temperature characteristics of the infiltration, agitation, nitrogen flushing, evacuation, and carbonation phases to identify a viable path to development of an optimized process suitable for scale-up to commercial implementation. The ultrasonic study has shown that sonication can be reduced from hours to seconds. The authors believe that there is a potential for this process to be scaled, and a pellet form of sorbent holds promise in the landscape of DAC technologies.

■ ASSOCIATED CONTENT

Supporting Information

The Supporting Information is available free of charge at https://pubs.acs.org/doi/10.1021/acsomega.4c03551.

Types of sonication used in production of PEI pellets; steps in the pellet synthesis process; press used for the pellet production process; experimental setup used for sonication; experimental setup used for purging; pellets prepared using the baseline process; freeze-fractured sample surface; FTIR spectra for pellets of different PEI loadings; and model fitting data for CO_2 uptake (PDF)

■ AUTHOR INFORMATION

Corresponding Author

Gregory P. Dillon − *School of Engineering, Penn State Erie, The Behrend College, Erie, Pennsylvania 16563, United States;* orcid.org/0000-0001-9839-8544; Email: gpd2@psu.edu

Author

Ramesh B. Komma − *School of Engineering, Penn State Erie, The Behrend College, Erie, Pennsylvania 16563, United States*

Complete contact information is available at: https://pubs.acs.org/10.1021/acsomega.4c03551

Author Contributions

†R.K. and G.D. contributed equally to this paper.

Notes

The authors declare no competing financial interest.

■ ACKNOWLEDGMENTS

The authors acknowledge the support of the Schools of Engineering and Science at Penn State Erie, The Behrend College, as well as the James R. Meehl Science and Engineering research fund. The authors also acknowledge the assistance of Clark Moose and Steven Struble Penn State's Applied Research for their kind assistance in completing the ultrasonic testing.

■ REFERENCES

(1) Choi, S.; Drese, J. H.; Jones, C. W. Adsorbent materials for carbon dioxide capture from large anthropogenic point sources. *ChemSusChem* **2009**, *2* (9), 796−854.

(2) Drese, J. H.; Talley, A. D.; Jones, C. W. Aminosilica materials as adsorbents for the selective removal of aldehydes and ketones from simulated bio-oil. *ChemSusChem* **2011**, *4* (3), 379−385.

(3) Nomura, A.; Jones, C. W. Amine-functionalized porous silicas as adsorbents for aldehyde abatement. *ACS Appl. Mater. Interfaces* **2013**, *5* (12), 5569−5577.

(4) Belmabkhout, Y.; Serna-Guerrero, R.; Sayari, A. Adsorption of CO2-containing gas mixtures over amine-bearing pore-expanded MCM-41 silica: Application for gas purification. *Ind. Eng. Chem. Res.* **2010**, *49* (1), 359−365.

(5) Tailor, R.; Abboud, M.; Sayari, A. Supported polytertiary amines: Highly efficient and selective SO 2 adsorbents. *Environ. Sci. Technol.* **2014**, *48* (3), 2025−2034.

(6) Bollini, P.; Didas, S. A.; Jones, C. W. Amine-oxide hybrid materials for acid gas separations. *J. Mater. Chem.* **2011**, *21* (39), 15100−15120.

(7) Dutcher, B.; Fan, M.; Russell, A. G. Amine-based CO2 capture technology development from the beginning of 2013-A review. *ACS Appl. Mater. Interfaces* **2015**, *7* (4), 2137−2148.

(8) Xu, X.; Pejcic, B.; Heath, C.; Wood, C. D. Carbon capture with polyethylenimine hydrogel beads (PEI HBs). *J. Mater. Chem. A Mater.* **2018**, *6* (43), 21468−21474.

(9) Xu, X.; Yang, Y.; Acencios Falcon, L. P.; Hazewinkel, P.; Wood, C. D. Carbon capture by DEA-infused hydrogels. *Int. J. Greenh. Gas Control* **2019**, *88*, 226−232.

(10) Chaikittisilp, W.; Khunsupat, R.; Chen, T. T.; Jones, C. W. Poly(allylamine)-mesoporous silica composite materials for CO 2 capture from simulated flue gas or ambient air. *Ind. Eng. Chem. Res.* **2011**, *50* (24), 14203−14210.
(11) Sakwa-Novak, M. A.; Tan, S.; Jones, C. W. Role of Additives in Composite PEI/Oxide CO2 Adsorbents: Enhancement in the Amine Efficiency of Supported PEI by PEG in CO2 Capture from Simulated Ambient Air. *ACS Appl. Mater. Interfaces* **2015**, *7* (44), 24748−24759.
(12) Goeppert, A.; Zhang, H.; Czaun, M.; May, R. B.; Prakash, G. K. S.; Olah, G. A.; Narayanan, S. R. Easily regenerable solid adsorbents based on polyamines for carbon dioxide capture from the air. *ChemSusChem* **2014**, *7* (5), 1386−1397.
(13) Pang, S. H.; Lee, L. C.; Sakwa-Novak, M. A.; Lively, R. P.; Jones, C. W. Design of Aminopolymer Structure to Enhance Performance and Stability of CO2 Sorbents: Poly(propylenimine) vs Poly(ethylenimine). *J. Am. Chem. Soc.* **2017**, *139* (10), 3627−3630.
(14) Zerze, H.; Tipirneni, A.; McHugh, A. J. Reusable poly-(allylamine)-based solid materials for carbon dioxide capture under continuous flow of ambient air. *Separ. Sci. Technol.* **2017**, *52* (16), 2513−2522.
(15) McDonald, T. M.; Lee, W. R.; Mason, J. A.; Wiers, B. M.; Hong, C. S.; Long, J. R. Capture of carbon dioxide from air and flue gas in the alkylamine-appended metal-organic framework mmen-Mg 2(dobpdc). *J. Am. Chem. Soc.* **2012**, *134* (16), 7056−7065.
(16) Sayari, A.; Liu, Q.; Mishra, P. Enhanced adsorption efficiency through materials design for direct air capture over supported polyethylenimine. *ChemSusChem* **2016**, *9* (19), 2796−2803.
(17) Sehaqui, H.; Gálvez, M. E.; Becatinni, V.; cheng Ng, Y.; Steinfeld, A.; Zimmermann, T.; Tingaut, P. Fast and reversible direct CO2 capture from air onto all-polymer nanofibrillated cellulose-polyethylenimine foams. *Environ. Sci. Technol.* **2015**, *49* (5), 3167−3174.
(18) Panda, D.; Kumar, E. A.; Singh, S. K. Amine Modification of Binder-Containing Zeolite 4A Bodies for Post-Combustion CO2 Capture. *Ind. Eng. Chem. Res.* **2019**, *58* (13), 5301−5313.
(19) Uehara, Y.; Karami, D.; Mahinpey, N. CO2 adsorption using amino acid ionic liquid-impregnated mesoporous silica sorbents with different textural properties. *Microporous Mesoporous Mater.* **2019**, *278*, 378−386.
(20) Zhang, W.; Gao, E.; Li, Y.; Bernards, M. T.; He, Y.; Shi, Y. CO2 capture with polyamine-based protic ionic liquid functionalized mesoporous silica. *J. CO2 Util.* **2019**, *34*, 606−615.
(21) Zhao, D.; Huo, Q.; Feng, J.; Chmelka, B. F.; Stucky, G. D. Nonionic Triblock and Star Diblock Copolymer and Oligomeric Surfactant Syntheses of Highly Ordered, Hydrothermally Stable, Mesoporous Silica Structures. *J. Am. Chem. Soc.* **1998**, *120*, 6024−6036.
(22) Knowles, G. P.; Liang, Z.; Chaffee, A. L. Shaped polyethyleneimine sorbents for CO2capture. *Microporous Mesoporous Mater.* **2017**, *238*, 14−18.
(23) Wijesiri, R. P.; Knowles, G. P.; Yeasmin, H.; Hoadley, A. F. A.; Chaffee, A. L. CO 2 Capture from Air Using Pelletized Polyethylenimine Impregnated MCF Silica. *Ind. Eng. Chem. Res.* **2019**, *58* (8), 3293−3303.
(24) Brunauer, S.; Emmett, P. H.; Teller, E. Adsorption of Gases in Multimolecular Layers. *J. Am. Chem. Soc.* **1938**, *60* (2), 309−319.
(25) Joyner, L. G.; Barrett, E. P.; Skold, R. The Determination of Pore Volume and Area Distributions in Porous Substances. II. Comparison between Nitrogen Isotherm and Mercury Porosimeter Methods. *J. Am. Chem. Soc.* **1951**, *73* (7), 3155−3158.
(26) Holewinski, A.; Sakwa-Novak, M. A.; Jones, C. W. Linking CO2 Sorption Performance to Polymer Morphology in Amino-polymer/Silica Composites through Neutron Scattering. *J. Am. Chem. Soc.* **2015**, *137* (36), 11749−11759.
(27) Li, C.; Wang, X.; Yang, A.; Chen, P.; Zhao, T.; Liu, F. Polyethyleneimine-Modified Amorphous Silica for the Selective Adsorption of CO2/N2 at High Temperatures. *ACS Omega* **2021**, *6* (51), 35389−35397.
(28) ACS Materials. "SBA 15", https://www.acsmaterial.com/sba-15-20g.html (accessed June 15, 2022).

https://doi.org/10.1021/acsomega.4c03551
ACS Omega 2024, 9, 32881−32892